A CFD-FEM analysis for Anaconda WEC with mooring lines

Y. Huang, Q. Xiao, G. Idarraga, L. Yang, S. Dai, F. Abad, F. Brennan, S. Lotfian

Abstract— **To obtain a deeper understanding on the dynamic response of flexible tube wave energy converter (WEC) in realistic ocean environment, the Anaconda WEC with mooring lines is numerically modelled in this paper. A coupled numerical analysis tool based on computational fluid dynamics (CFD) and finite element analysis (FEA) method was established to perform fluid-structure interaction (FSI) simulations for Anaconda WEC. The surrounding flow is solved by a two-phase CFD solver, and the structural dynamics are calculated using a three-dimensional (3D) FEA code. Strong coupling between the fluid and solid phases is achieved by adopting a multi-physical coupling library. With this tool, the FSI responses of Anaconda WEC with mooring lines under regular waves can be captured. The tube motion, pressure field, generated power, structure deformation and stress distribution are fully examined to explore the impact of mooring line on the performance of the device. The results indicate that an increase in mooring line stiffness leads to a reduction in tube's bow motion, resulting in decreased internal pressure and reduced energy generation. A higher mooring line stiffness reduces the extent of variation of cross-sectional area, leading to a lower hoop stress and mitigating the risk of material failure.**

Keywords — **Flexible WEC, CFD, FEA, Fluid-Structure Interaction; Mooring Line.**

I. Introduction

Flexible wave energy converters (fWECs) have gained significant attention in recent years due to their exceptional adaptability to complex sea conditions and cost-effectiveness. A variety of fWEC designs have been proposed, and one notable example is the Anaconda WEC. It consists of a flexible tube and a PTO system at the stern, located near the wave surface. As waves pass over the device, the pressure difference across the tube changes, resulting in variations in the cross-sectional area and the generation of a bulge wave. This bulge wave propagates along the tube, converting the external wave energy into kinetic energy of the fluid inside the tube and ultimately being absorbed by the PTO located at the end of the tube [1].

One of the key features of fWECs is the utilization of flexible materials as the primary mover and the power take-off (PTO) system. The application of flexible materials has made the hydro-elastic responses more complex. To investigate the complicated fluid-structure interaction (FSI) characteristics of fWECs, a series of wave tank tests have been conducted [2-4]. Chaplin et al. [2] and Heller et al. [3] tested a 1:25 scale model of the Anaconda WEC, with both ends fixed, to study its response in calm water and regular waves. The prediction of distensibility of the flexible agreed well with experimental data. The capture width was found to be optimal when the bulge wave speed was close to the external water wave speed. The influence of PTO impedance on the power generation of Anaconda WEC was also discussed. Mendes et al. [4] performed wave tank tests on a 1:50 scale Anaconda model, with one end fixed and the other end free, to assess its responses under regular waves. The PTO system was considered via an orifical plate with varying diameters. The resonant phenomena were observed not only when the bulge wave speed matched the water wave speed but also when the incident wave frequency was equal to the OWC natural frequency.

Additionally, numerical simulations based on reduced order models are also performed to investigate the FSI responses of fWECs. Farley et al. [5] proposed a one-dimensional dynamic model for numerical modelling of the Anaconda WEC using homogeneous flexible materials.

Y. Huang is with Department of Naval Architecture, Ocean and Marine Engineering, University of Strathclyde, Glasgow, UK (email: y.huang@strath.ac.uk).

Q. Xiao is with Department of Naval Architecture, Ocean and Marine Engineering, University of Strathclyde, Glasgow, UK (email: qing.xiao@strath.ac.uk) (corresponding author).

G. Idarraga is with Department of Mechanical and Aerospace Engineering, University of Strathclyde, Glasgow, UK (email: g.idarraga@strath.ac.uk).

L. Yang is with Department of Mechanical and Aerospace Engineering, University of Strathclyde, Glasgow, UK (email: l.yang@strath.ac.uk).

S. Dai is with Department of Naval Architecture, Ocean and Marine Engineering, University of Strathclyde, Glasgow, UK (email: saishuai.dai@strath.ac.uk).

F. Abad is with Department of Naval Architecture, Ocean and Marine Engineering, University of Strathclyde, Glasgow, UK (email: farhad.abad@strath.ac.uk).

F. Brennan is with Department of Naval Architecture, Ocean and Marine Engineering, University of Strathclyde, Glasgow, UK (email: feargal.brennan@strath.ac.uk).

S. Lotfian is with Department of Naval Architecture, Ocean and Marine Engineering, University of Strathclyde, Glasgow, UK (email: saeid.lotfian@strath.ac.uk).

This is a peer-reviewed, accepted author manuscript of the following paper: Huang, Y., Xiao, Q., Idarraga, G., Yang, L., Dai, D., Abad, F., Brennan, F., & Lotfian, S. (Accepted/In press). A CFD-FEM analysis for Anaconda WEC with mooring lines. In Proceedings of the 15th European Wave and Tidal Energy Conference 2023 [163] EWTEC.

A variety of wave frequencies were considered, and the bulge of flexible tube was found to grow linearly with distance at resonance. Chaplin et al. [2] extended the above model and applied it to simulate Anaconda WEC with heterogeneous material, where the tube is reinforced with inextensible fibres in longitudinal direction. Two ends of the tube were fixed in the simulation. In addition, Babarit et al. [6] developed a linear numerical model based on linear potential flow theory and linearised wall equation for analysing the dynamic responses of flexible tube WEC. Different with the model of Chaplin et al. [2], the surge motion of the tube was taken into account, while the other degree-of-freedom (DoF) motions were ignored.

It is noted that most of the undertaken research assumes that both ends of Anaconda model are fixed, neglecting mooring lines that do exist in real conditions. When mooring lines are considered, the tube is allowed to move head to waves. This is evident by an experiment conducted by Checkmate Flexible Engineering Ltd., where they observed a significant heave motion of Anaconda WEC, which may impact the dynamic response of WEC and further the energy conversion [7]. In addition, most of the existing reduced order models proposed for Anaconda WEC do not incorporate the motion, thereby failing to account for the influence of mooring lines.

This study is a follow up of our previous analysis on an Anaconda WEC using CFD-FEA method [8]. It extends to the examinations on a fWEC system from the existing without mooring line to adding mooring at the bow of tube. The main objective is the advancement of novel wave-structure interaction simulation applicable to the flexible tube WECs to predict the wave-flexible material-structure behaviour of fWECs subjected to multiple degree of freedom which is caused by mooring system.

II. Numerical Method

A fully coupled FSI analysis tool based on CFD and FEA method is established to simulate the responses of flexible WEC. The surrounding flow around the WEC is resolved by solving three-dimensional incompressible Navier-Stokes (N-S) equations with finite volume approach. The structure dynamics is obtained by solving the weak form of momentum equations using finite element approach. Strong coupling between fluid and solid is considered.

A CFD solver developed based on OpenFOAM is selected to model the two-phase flow around the WEC [9]. The governing equations of fluid include the continuity equation and N-S equations, given as:

$$\nabla \cdot \mathbf{U} = 0 \tag{1}$$

$$\frac{\partial(\rho \mathbf{U})}{\partial t} + \nabla \cdot (\rho(\mathbf{U} - \mathbf{U}_g))\,\mathbf{U} = -\nabla p_d - \mathbf{g} \cdot x \nabla \rho + \nabla \cdot (\mu \nabla \mathbf{U}) + (\nabla \mathbf{U}) \cdot \nabla \boldsymbol{\mu} + \boldsymbol{f}_\sigma + \boldsymbol{f}_p \tag{2}$$

where $\mathbf{U}$ is the flow velocity. $\mathbf{U}_g$ represents the velocity of grid node, resulted from the dynamic mesh. ρ denotes the mixture density of multi-phase flow. p_d is the dynamic pressure. $\mathbf{g}$ is gravity acceleration vector. μ is the dynamic viscosity. $\boldsymbol{f}_\sigma$ and $\boldsymbol{f}_p$ are source terms that represent the surface tension and porous media, respectively. The volume of fluid approach is utilized to capture the free surface. The PIMPLE algorithm is used to solve N-S equations. A laminar model is adopted to simulate the low Reynolds number flows.

An opensource 3D FEM code is chosen to obtain the structural dynamics of the flexible WEC [10]. The governing equation for structure is described by:

$$\boldsymbol{\rho_s} \frac{\boldsymbol{D^2 \mathrm{U}_s}}{\boldsymbol{D^2 t^2}} = \boldsymbol{\nabla} \cdot \mathbf{P} + \boldsymbol{\rho_s} \mathbf{f} \tag{3}$$

where ρ_s is the density of the structure.$\mathbf{U}_s$ represents the displacement vector. $\mathbf{P}$ denotes the second Piola–Kirchoff stress tensor, used to calculate the surface force. $\mathbf{f}$ is the body force of pre-unit mass, such as gravity. The finite element method is used to discretize the above structure governing equation. The discretization in the time domain is completed using α-method [11].

A strong coupling approach with a partitioned scheme is applied to achieve the coupling between the fluid and solid phases [12]. A schematic diagram of the simplified coupling procedure is shown in Fig. 1. During the FSI simulation, the forces calculated from the fluid solver are transferred to the structural solver. Conversely, the displacements obtained by the structural solver are passed back to the fluid solver. Additionally, an improved IQN-ILS approaches is applied to stabilize the calculation and accelerate the convergence progress.

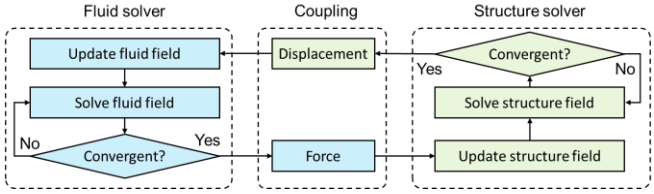

Fig. 1 schematic diagram of coupling between fluid and solid phases

III. Problem Description

A. Geometry model

The Anaconda WEC model studied in this work is based on the experiment conducted by Mendes et al. [4]. As shown in Fig. 2, the model is composed of a horizontal flexible rubber tube, an elbow and a rigid vertical tube. In the experiment, the bow of flexible tube is free to move without any constrains, and the stern of flexible tube is connected to the fixed rigid vertical tube. In the present simulation, the mooring line is represented by a spring with different stiffness to restrict the motion of the flexible tube. The spring is arranged horizontally with a length of 1m, which is connect to the bow of the flexible tube. The geometry dimensions of the rubber tube are summarized in Table 1. The Young's modulus and Poisson ratio of the rubber is 0.91 MPa and 0.5, respectively. The tube is filled with water, and the initial water elevation inside the right vertical tube is 0.23 m above the external free surface, providing a static hydrodynamic pressure of 2312 Pa in the flexible tube.

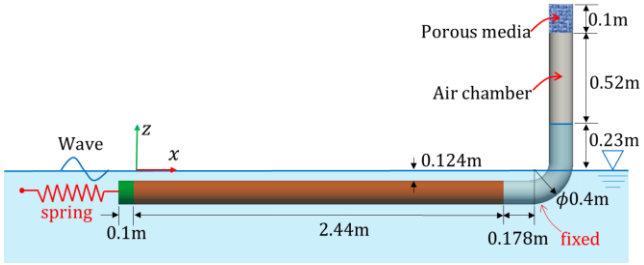

Fig. 2 Schematic diagram of the Anaconda WEC model

TABLE I
GEOMETRY DIMENSIONS OF FLEXIBLE RUBBER TUBE

Length (L)	Diameter (D)	Thickness (t)
2.44 m	0.1654 m	2 mm

B. PTO impedance

To model the PTO impedance, a porous media with a hight of 0.1 m is set near the top of the vertical tube, as shown in Fig. 2. A source term $\boldsymbol{f_p}$ is added to the governing equations to consider the influence of PTO, as indicated in Eq. (2). Additionally, $\boldsymbol{f_p}$ is defined by the following equation [13]:

$$\boldsymbol{f_p} = -(\mu D + \frac{1}{2}\rho|U|F)\,\boldsymbol{U} \tag{4}$$

where D and F are coefficients related to the physical properties of the porous media. A homogeneous porous media with linear damping is used in this study, therefore F is set to 0. In addition, D is set as 2e10 to provide a large PTO impedance.

C. Bulge wave speed

According to the study of Chaplin et al. [2], the resonant responses occur when the bulge wave speed (c_b) matches the external water wave speed (c_g). The bugle wave speed c_b is determined by the properties of flexible rubber tube, which can be obtained by the following equations:

$$c_b = 1/\sqrt{\rho_l D_t} \tag{5}$$

$$D_t = (1/S)/(\partial S/\partial p) \tag{6}$$

where ρ_l is the density of fluid inside the tube. D_t is the distensibility of rubber tube. S and p represent the cross-sectional area and pressure inside the tube, respectively. In this study, the calculated bulge wave speed of flexible rubber tube is 3.82 m/s.

D. Numerical studies

Fig. 3 shows a three-dimensional computational domain for this study. The model is placed in the centre of the domain, with 1m from the inlet boundary. The fluid mesh and structure mesh are presented in Fig. 4. The total grid number of fluid mesh is around 1.06 million. To better capture the wave profile and calculate the tube deformation, the mesh near the air and water free surface and flexible tube is refined, as shown in Fig. 4(a). The velocity and pressure boundary conditions of the Anaconda model are set to non-slip wall and zero gradient, respectively. For the inlet boundary, the velocity and pressure are prescribed by the wave theory. The velocity and pressure boundary conditions at the outlet boundary are both set to zero gradient. Additionally, symmetry conditions are applied to the sidewalls of the computational domain. To perform the structural analysis, 600 quadratic brick elements are used for the flexible tube, as shown in Fig. 4(b).

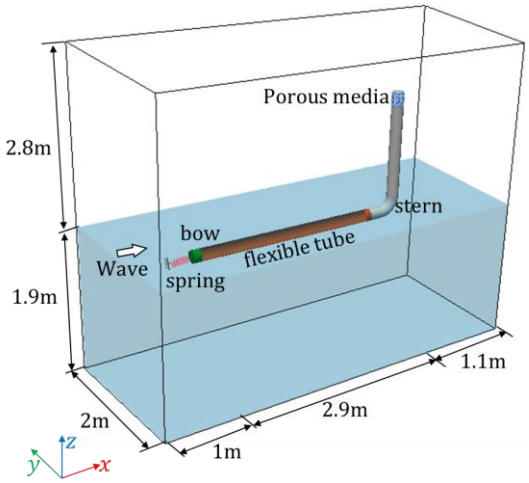

Fig. 3 Computational domain

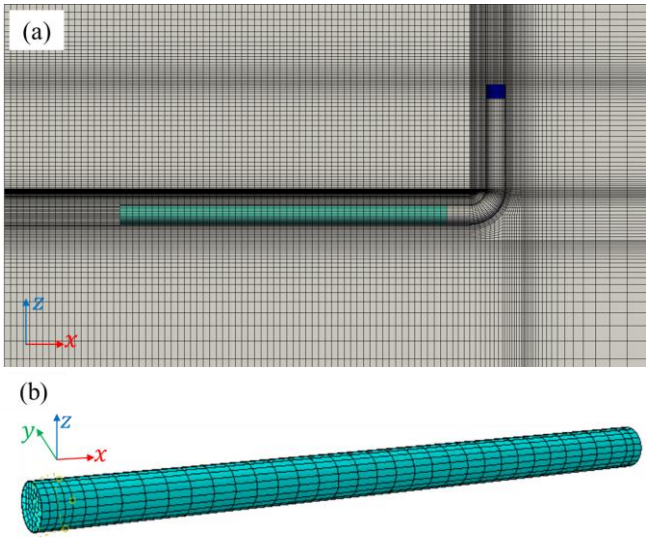

Fig. 4 Mesh distribution: (a) fluid mesh, the region marked out with blue colour represents the porous media; (b) structure mesh.

In this study, regular waves are selected as the incident wave condition with the wave amplitude (A_W) of 0.05 m. To allow the resonant response to occur, the wave speed is set as 3.82 m/s, equal to the bugle wave speed mentioned above. The corresponding wave period (T_W) is 3.33 s. The impact of mooring on the device dynamics is studied via varying stiffness (k) of spring as listed in Table 2. Due to the lack of experimental data, the stiffness of the mooring lines is determined based on the experimental study of a floating platform with mooring lines [14]. In the subsequent discussions, 'fixed' and 'free' are denoted to Case 1 & 5 in which no mooring lines are imposed. The remaining cases are with mooring lines at different stiffnesses.

In this study, the x-direction DoF is restricted, meaning that the displacement of the tube in the x-direction is not considered. This is due to two reasons. The wave tank test

conducted by Mendes et al. indicated that the displacement of the flexible tube along x-direction is negligible [4]. On the other hand, fixing the x-direction DoF enhances the stability of FSI simulation.

TABLE II
SUMMARY OF NUMERICAL CASES

No.	Tube bow	Stiffness k (kN/m)
Case 1	Free, without mooring line	-
Case 2	Constrained by mooring line	25
Case 3	Constrained by mooring line	50
Case 4	Constrained by mooring line	75
Case 5	Fixed, without mooring line	-

IV. RESULTS

The simulation results will be presented in this section starting with the bulge wave. The displacement of tube bow, internal pressure and capture width are then examined to explore the impact of mooring. The structure responses of the flexible tube, such as the deformed shape and hoop strain, are also investigated.

A. Bulge wave

One of the most prominent characteristics of the Anaconda WEC is the bugle wave. When external water waves pass over the flexible tube, it induces a pressure difference across the tube wall, resulting in the variation in the cross-sectional area of the tube, given a name of "bulge". The bulge wave carries wave energy from the bow to the stern, facilitating its absorption by the PTO at the end of the tube. Fig. 5 illustrates the simulation results showing the variation of cross-sectional area $S(x,t)$ of the tube along its length over one wave period when the tube's bow freely moves. The largest variation of $S(x,t)$ occurs at the end of the tube, which is a typical characteristic when the resonance occurs. The time history of $S(x,t)$ at $x/L = 0.9$ is examined to explore the influence of mooring line, as shown in Fig. 6. It can be seen that the maximum $S(x,t)$ appears for 'free' condition, indicating an adverse impact of the mooring line on the cross-sectional area variation.

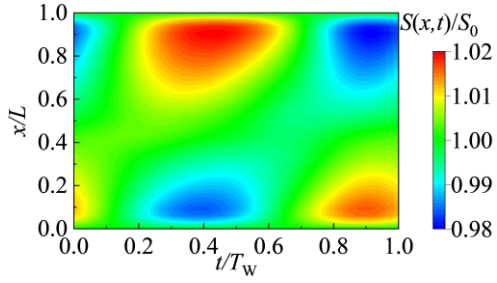

Fig. 5 Variation of the cross-sectional area of the tube along its length over one wave period.

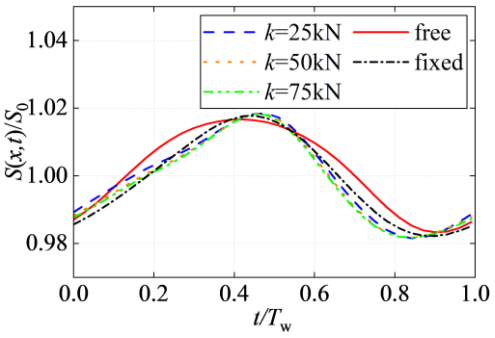

Fig. 6 Time history of cross-sectional area at x/L = 0.9 over one wave period.

B. Flow field

The motion of flexible tube is greatly affected by the mooring line, as shown in Fig. 7. Only displacements in y (sway) and z (heave) directions are shown in the figure since the x-direction DoF is fixed. The displacement of tube's bow in z direction (d_Z) is much larger than that of y direction (d_Y). Additionally, increasing k results in a significant reduction in the motion at the bow, further leads to the pressure variation inside the tube. Previous studies revealed that the maximum pressure fluctuation appears at the tube stern when the resonance occurs [2, 8]. Since the pressure is observed almost uniformly distributed across tube, therefore, we plot the time history of pressure at the centre point of the cross-section at tube's stern (x/L = 1) as shown in Fig. 8. Compared to a 'fixed' condition, the pressure fluctuation increases by 8% when the tube's bow is allowed to move freely without the constrains of mooring. Furthermore, the periodic pressure variation at the tube's stern drives water column moves up and down inside the vertical tube, thereby altering the pressure inside the air chamber and allowing wave energy to be absorbed by the PTO located at the top of the vertical tube. Fig. 9 presents the time history of water elevation in vertical tube. Clearly, the variation of water level is very similar for different k, with a maximum difference of 7%. The pressure within the air chamber is summarized in Table 3, indicating a pressure increases by 8% under 'free' condition. The pressure field plotted in Fig. 10 for 'free' condition indicates that the pressure distribution is almost uniform in the air chamber at different instants. Although the vertical pipe is open to air, the pressure oscillation amplitude inside the air chamber is significantly higher than the pressure variation of the surrounding fluid due to the blocking effect of the porous media.

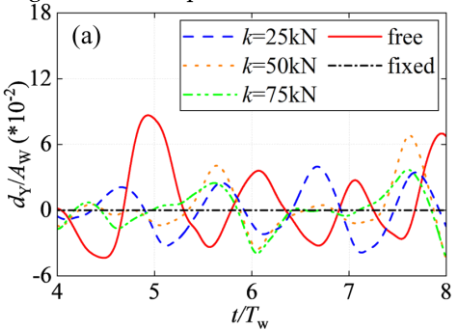

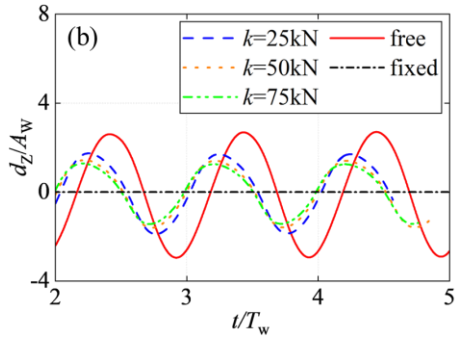

Fig. 7 Time history of tube bow displacement: (a) d_Y, the displacement in the y direction; (b) d_Z, the displacement in the z direction.

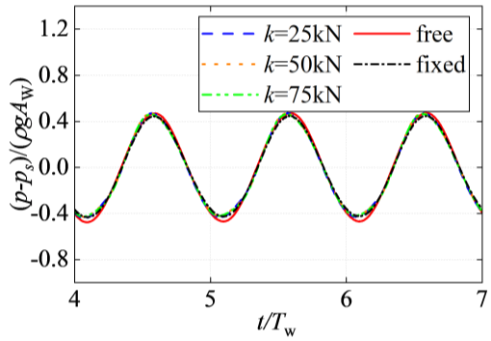

Fig. 8 Time history of pressure (p) at the centre point of the cross-section at the stern of flexible tube (x/L = 1), p_s = 4355 Pa is the hydrostatic pressure at the corresponding position.

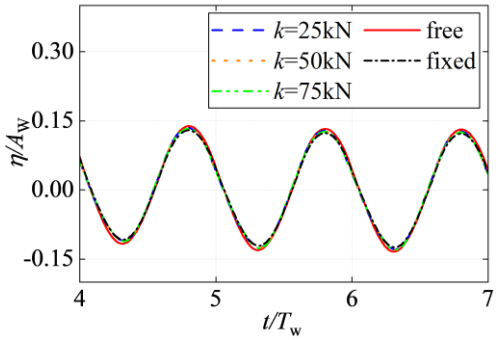

Fig. 9 Time history of water elevation (η) in the vertical tube.

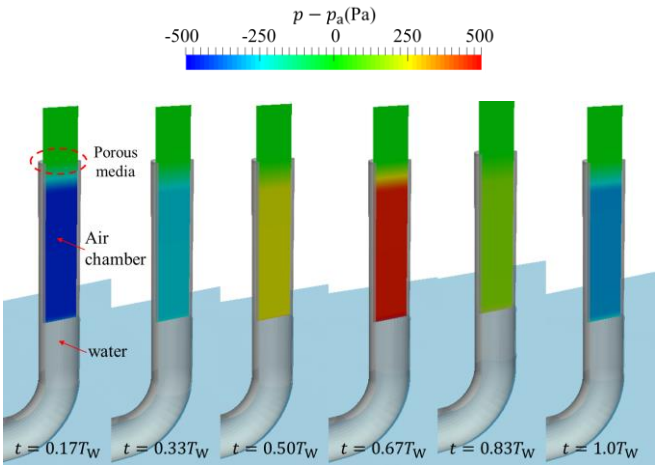

Fig. 10 Pressure field (p) in the air chamber at different instants over one wave period under 'free' condition, p_a denotes the atmospheric pressure.

C. *Generated power*

To further explore the impact of mooring line on the power generation, the magnitudes of capture power (*CW*) are calculated by the following equations:

$$W = \int_0^{T_w} p(t)Q(t)\mathrm{d}t \quad (7)$$

$$CW = W / \frac{1}{2}\rho_l g {A_W}^2 C_g \quad (8)$$

where W represents the power absorbed by the PTO. p is the volume-averaged pressure in the air chamber. $Q(t)$ denotes the volume flux across the porous media.

Table 4 summarizes the $Q(t)$ across the porous media and Fig. 10 plot the CW normalized by the tube diameter (D) for different conditions. As the mooring stiffness decreases, $Q(t)$ increases and CW gradually increases, indicating that the motion of the tube's bow benefits the energy absorption. Compared to a fixed bow, the CW increases by 15% when the tube's bow freely moves without mooring line.

TABLE III
PRESSURE AT THE WATCH POINT (Z = 0.7 M) INSIDE THE AIR CHAMBER

Cases	Mean value $\bar{p} - p_a$ (Pa)	Amplitude (Pa)
Free	0.0	468.8
k = 25 kN	0.0	454.1
k = 50 kN	0.0	452.6
k = 75 kN	0.0	448.9
Fixed	0.0	435.4

p_a is the atmospheric pressure.

TABLE IV
VOLUME FLUX ACROSS THE POROUS MEDIA

Cases	Mean value (cm^3/s)	Amplitude (cm^3/s)
Free	0.0	244.2
k = 25 kN	0.0	233.9
k = 50 kN	0.0	231.4
k = 75 kN	0.0	228.9
Fixed	0.0	228.4

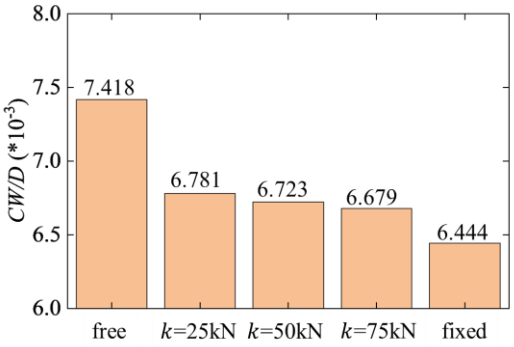

Fig. 10 Capture width of the Anaconda WEC model under different mooring line stiffness conditions.

D. *Structural deformation*

The $S(x,t)$ of the tube along the tube length are plotted in Fig. 11 for different k. The deformed shapes of the tube are almost the same regardless of k. The maximum $S(x,t)$ appears at both ends of the tube. The hoop stress of the cross-section at x/L = 0.9 is plotted in Fig. 12. It can be observed that as k decreases, the stress gradually increases, resulted from a larger variation of

$S(x,t)$. The instantaneous von-stress distribution of flexible tube, presented in Fig. 13, reveals that a lager von-stress at the stern of tube is observed for 'free' condition, indicating a higher risk of structural failure.

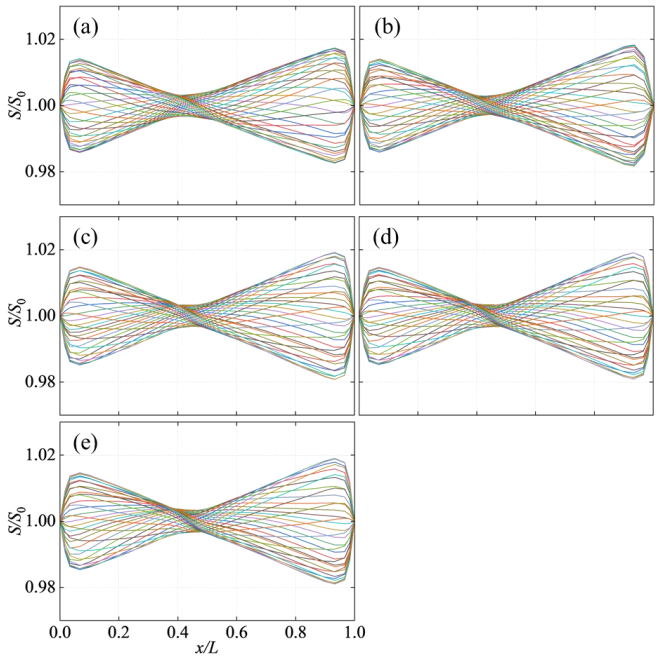

Fig. 11 Cross-sectional area plotted over the tube length at 32 instants over one wave period: (a) fixed; (b) free; (c) k = 25 kN; (d) k = 50 kN; (e) k = 75 kN.

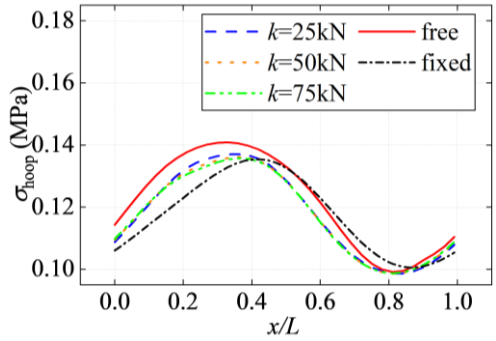

Fig. 12 Time history of the hoop stress of the cross-section at x/L =0.9.

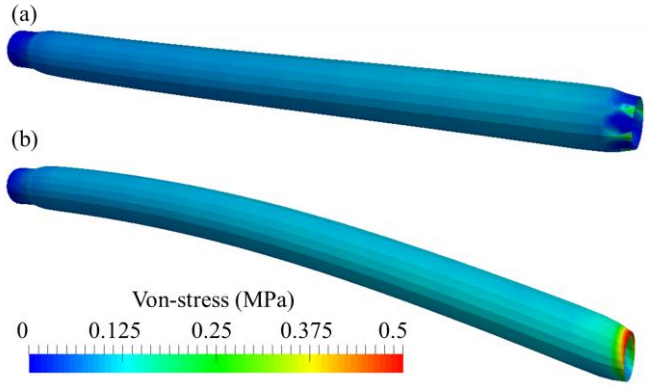

Fig. 13 Instantaneous (t/T_W = 0.25) von-stress distribution on the flexible tube under different conditions: (a) 'fixed'; (b) 'free'.

V. CONCLUSIONS

The present work aims at studying the impact of mooring line on the fluid-structure interaction responses of Anaconda WEC. A coupled CFD-FEA tool is established for the FSI simulation of Anaconda WEC in regular waves. The CFD results successfully capture the bulge wave and resonant responses of device. Moreover, it is found that increasing the stiffness of the mooring line reduces the motion of tube's bow, resulting in a decrease in internal pressure and a reduction in energy generation. Additionally, higher mooring stiffness reduces the extent of variation of cross-sectional area, leading to a decrease in hoop strain and mitigating the risk of material failure. Future work will focus on integrating electrical field simulation into the existing FSI analysis tool, enabling the simulation of flexible WECs using DEGs as PTO systems, while considering the impact of electric field on the deformation of flexible material.

ACKNOWLEDGEMENT

This research was supported by an EPSRC Grant "Bionic Adaptive Stretchable Materials for WEC (BASM-WEC)" (No. EP/V040553/1). This work used the Cirrus UK National Tier-2 HPC Service at EPCC (http://cirrus.ac.uk) funded by the University of Edinburgh and EPSRC (EP/P020267/1).

REFERENCES

[1] Farley, F. J. M., & Rainey, R. C. T. (2011). U.S. Patent No. 7,980,071. Washington, DC: U.S. Patent and Trademark Office.

[2] Chaplin, J. R., Heller, V., Farley, F. J. M., Hearn, G. E., & Rainey, R. C. T. (2012). Laboratory testing the Anaconda. Philosophical Transactions of the Royal Society A: Mathematical, Physical and Engineering Sciences, 370(1959), 403-424.

[3] Heller, V., Chaplin, J. R., Farley, F. J. M., Hann, M. R., & Hearn, G. E. (2000, May). Physical model tests of the anaconda wave energy converter. In Proc. 1st IAHR European Congress.

[4] Mendes, A. C., Braga, F. P., Paredes, L. M. A., & Chaplin, J. R. (2017, June). Performance assessment of the ANACONDA WEC in regular waves at 1: 50 model scale. In International Conference on Offshore Mechanics and Arctic Engineering (Vol. 57786, p. V010T09A016). American Society of Mechanical Engineers.

[5] Farley, F. J. M., Rainey, R. C. T., & Chaplin, J. R. (2012). Rubber tubes in the sea. Philosophical Transactions of the Royal Society A: Mathematical, Physical and Engineering Sciences, 370(1959), 381-402.

[6] Babarit, A., Singh, J., Mélis, C., Wattez, A., & Jean, P. (2017). A linear numerical model for analysing the hydroelastic response of a flexible electroactive wave energy converter. Journal of Fluids and Structures, 74, 356-384.

[7] Checkmate Flexible Engineering, https://www.checkmateukseaenergy.com/, accessed 15th December 2022.

[8] Huang, Y., Xiao, Q., Idarraga, G., Yang, L., Dai, S., Ahad, F., Brennan, F., Lotfian, S. (2023, June). Numerical analysis of flexible tube wave energy converter using CFD-FEA method. In International Conference on Offshore Mechanics and Arctic Engineering (OMAE2023-101302). American Society of Mechanical Engineers (OMAE-101302, accepted).

[9] Jasak, H., Jemcov, A., & Tukovic, Z. (2007, September). OpenFOAM: A C++ library for complex physics simulations. In International workshop on coupled methods in numerical dynamics (Vol. 1000, pp. 1-20).

[10] Dhondt, G. (2017). Calculix crunchix user's manual version 2.12. Munich, Germany, accessed Sept, 21, 2017.

[11] Luo, Y., Xiao, Q., Shi, G., Wen, L., Chen, D., & Pan, G. (2019). A fluid–structure interaction solver for the study on a passively deformed fish fin with non-uniformly distributed stiffness. Journal of Fluids and Structures, 92, 102778.

[12] Bungartz, H. J., Lindner, F., Gatzhammer, B., Mehl, M., Scheufele, K., Shukaev, A., & Uekermann, B. (2016). preCICE–a fully parallel library for multi-physics surface coupling. Computers & Fluids, 141, 250-258.

[13] Barree, R. D., & Conway, M. W. (2004, September). Beyond beta factors: a complete model for Darcy, Forchheimer, and trans-Forchheimer flow in porous media. In SPE annual technical conference and exhibition. OnePetro.

[14] Leroy, V., Delacroix, S., Merrien, A., Bachynski-Polić, E. E., & Gilloteaux, J. C. (2022). Experimental investigation of the hydro-elastic response of a spar-type floating offshore wind turbine. Ocean Engineering, 255, 111430.